









## Research Article

# Analysis of Different PWM Techniques for Enhanced Ultrahigh Gain Z-Network Topology

Vadthya Jagan <sup>1</sup>, Bhavadish Chary Maheshwaram <sup>1</sup>, Mallesh Usirikapally <sup>1</sup>,  
Praveen Kumar Balachandran <sup>2</sup>, B. Nagi Reddy <sup>1</sup>, Sankeerthana Mettu <sup>1</sup>,  
C. Dhanamjayulu <sup>3</sup>, G. Arunkumar,<sup>3</sup> K. C. Saranya,<sup>3</sup> and Baseem Khan <sup>4,5</sup>

<sup>1</sup>Department of Electrical and Electronics Engineering, Vignana Bharathi Institute of Technology, Hyderabad, India

<sup>2</sup>Department of Electrical and Electronics Engineering, Vardhaman College of Engineering, Hyderabad, India

<sup>3</sup>School of Electronics Engineering, Vellore Institute of Technology, Vellore, India

<sup>4</sup>Department of Electrical and Computer Engineering, Hawassa University, Hawassa 05, Ethiopia

<sup>5</sup>Department of Electrical and Electronic Engineering Technology, Faculty of Engineering and the Built Environment, University of Johannesburg, Johannesburg, South Africa

Correspondence should be addressed to Baseem Khan; [bkhan04021987@gmail.com](mailto:bkhan04021987@gmail.com)

Received 11 May 2023; Revised 14 September 2023; Accepted 2 December 2023; Published 6 February 2024

Academic Editor: Faroque Azam

Copyright © 2024 Vadthya Jagan et al. This is an open access article distributed under the Creative Commons Attribution License, which permits unrestricted use, distribution, and reproduction in any medium, provided the original work is properly cited.

In these modern times, the Z-source inverters (ZSIs) have become a revolutionary invention ever since the year 2002. The pulse-width modulation (PWM) technique used for most of the ZSIs is simple boost control PWM (SBC-PWM), and the SBC-PWM implies for a greater voltage stress on the inverter bridge and provides less boost factor. Likewise, many topologies for the basic Z-source topologies are evolved, and different PWM techniques are applied to them such as maximum boost control (MBC), maximum boost control with third harmonic injection (MBC-THI), maximum constant boost control (MCBC), and constant boost control with third harmonic injection (CBC-THI). All these mentioned PWM techniques are compared, and the converter opted in this paper is an enhanced ultrahigh gain active-switched quasi-Z-source inverter (EUHG-qZSI). The comparisons discussed in this brief are bridge stress, voltage gain, and voltage boost variation under each control strategy implementation. The theoretical and simulation evaluation for the abovementioned findings is presented in this paper, and the best PWM among them is maximum boost control (MBC).

## 1. Introduction

The inverters are basic power electronic converters which are used for the DC-AC conversion by using a proper switching strategy. The first ever inverter introduced was the voltage source inverter (VSI). In the voltage source inverter, the switching strategy used for controlling the inverter bridge is the pulse-width modulation (PWM) technique [1]. In these PWM techniques, there are various PWM techniques such as the single-pulse-width modulation (SPWM), multiple-pulse-width modulation (MPWM), and sinusoidal-pulse-width modulation (sine PWM). Using these basic PWM techniques, the VSIs are controlled accordingly. But this traditional inverter has permissible limitations, such as VSI acts as

the buck inverter, whereas the current source inverter (CSI) acts as a boost inverter and vice versa of the abovementioned criterion is not possible [2]. The switches in a leg of CSI cannot be opened at the same time. The buck-boost operation is not relatable in these traditional inverter topologies.

Hence, the Z-source inverter (ZSI) was introduced in the year 2003 [3]. This inverter was introduced to acquire higher voltage gain with low input value. The dead short circuit or shoot-through state of VSI is convoluted into an advantage in ZSI, under shoot-through state (ST), and the inductor-capacitor ( $L$ - $C$ ) pair stores energy and dissipates them in the form of boost under non-shoot-through state (NST). In the practical case, one must create the shoot-through to acquire the voltage boost. This criterion is not possible with the basic

PWM techniques. Thus, other PWM techniques were introduced in later times, and one such technique implemented for ZSI is the simple boost control technique (SBC).

This technique permits ST condition under inverter operation which leads to voltage boost in the output; boost depends on the ST period of the inverter bridge. Hence, to control the boosting terminology, one must control the duty ratio of inverter switches. The SBC leads to higher voltage stress on the inverter bridge under operation [3]. To overcome this limitation, various PWM techniques such as maximum boost control (MBC) [4], maximum boost control with third harmonic injection (MBC-THI) [4], maximum constant boost control (MCBC) [5], and constant boost control with third harmonic injection (CBC-THI) [5] and many more techniques were introduced in later times. Also, the SBC control scheme was implemented to EB-qZSI topology [6]. Likewise, the MCBC was initially implemented and analyzed with enhanced ultrahigh gain active-switched Z-source topology [7]. The MBC was implemented for the switched inductor Z-network topology [8]. The CBC-THI control technique was explained and illustrated with the basic Y-source inverter (YSI) in [9]. Later, the THI control scheme [4] was also implemented to the improved Z-source inverter topology [10], but the circuit is bulky. After this, a series of new control schemes were introduced [11], but these schemes are highly preferable for the single-phase PWM strategy. A space-vector modulation (ZSVM6) control strategy was introduced in [12] focusing on inductor current ripple reduction for qZSI topology. In recent times, a new discontinuous space vector modulation strategy is introduced, applied to ZSI topology [13], and this brief mainly focuses on the thermal stresses on the switches and also improves the inverter performance over harmonic content which can be done through regulating the modulation index. All over these, a novel strategy was introduced in [14] which is applied to the qSBI topology, but the gain value is satisfactory and limited to some applications only. Recently, extreme boost-quasi-Z-source inverters [15], switched quasi-impedance-source networks [16], and analysis of conventional PWM techniques for enhanced ultrahigh gain Z-network [17] are proposed.

This paper provides a comparative analysis between the five conventional PWM techniques illustrated in the earlier case. The analysis is performed by using a similar topology in every case. The topology chosen for comparative analysis is the enhanced ultrahigh gain active-switched-impedance quasi-Z-source inverter (EUHG-qZSI) [7]. These control strategies are applicable to each and every Z-network topology introduced ever since. In this brief, the comparative analysis is performed for five PWM techniques illustrated above. Under Section 1, the basic introduction for all five conventional PWM techniques is discussed. In Section 2, the methodology of five techniques and the operation of chosen topology are illustrated. The comparative analysis and the main idea are discussed briefly in Section 3. Under Section 4, the theoretical verification and analysis with simulation are discussed for the converter. The summarization and the acquired conclusions are discussed in Section 5.

## 2. Types of PWM Techniques

This section explains the traditional pulse-width modulated control techniques with their corresponding waveforms.

*2.1. Simple Boost Control [4].* The inverters are DC-AC converters which have huge applications in present generations. The inverters that fall under this era are traditional inverters, such as the voltage source inverter (VSI) and current source inverter (CSI). The traditional inverters are controlled by the traditional PWM techniques such as sine PWM and carrier-based PWM techniques. These inverters are operated as buck converter (VSI) and boost converter (CSI) according to the control scheme implemented. These traditional inverters are not buck-boost converters; hence, the impedance source inverter (ZSI) was introduced. When the traditional PWM is applied to the ZSI, it acts as a traditional inverter which means there is no boost in the output. Hence, the simple boost control technique (SBC) is introduced [4].

The first ever introduced PWM technique for the boosting terminology of the Z-source inverter is the simple boost control technique. This technique is designed to convert the shoot-through state vectors of traditional VSI to acquire a boost in the output voltage. This technique employs a three-phase reference signal enclosed by a straight line equal or greater than the peak value of the reference signal. The total envelope of signals is compared with the carrier wave or by triangular signal and is depicted in Figure 1(a). The same control strategy is possible with the single-phase sine signal, but the boosting ability is increased with three-phase signals. This control scheme is also implemented in EB-qZSI [6, 18] topology. The impedance network which is used in the inverter topology maintains the six active states unchanged as the traditional PWM technique, and in this technique, the obtainable shoot-through duty ratio,  $D$ , is increased, which increases voltage boost and the boost factor for the presented EUHG-qZSI [7] derived as follows:

$$B = \frac{2(1+D)}{1-5D-2D^2}, \quad (1)$$

where  $D$  is the shoot-through ratio and  $B$  is the boost factor. For an enhanced ultrahigh gain active-switched network q-ZSI (EUHG-qZSI) [7], the duty ratio is limited in the range of  $0 < D < 0.186$  as given in (1). The inverter output also depends on the modulation index,  $M$ . The variation in the modulation index,  $M$ , will vary the gain value of the topology. The voltage gain,  $G$ , value is given as

$$G = \frac{M \cdot B}{2}. \quad (2)$$

The relation between duty ratio,  $D$ , and modulation index,  $M$ , for the simple boost control technique is given as

$$D = 1 - M, \quad (3)$$

$$B = \frac{(2M-4)}{2M^2+9M+6}. \quad (4)$$

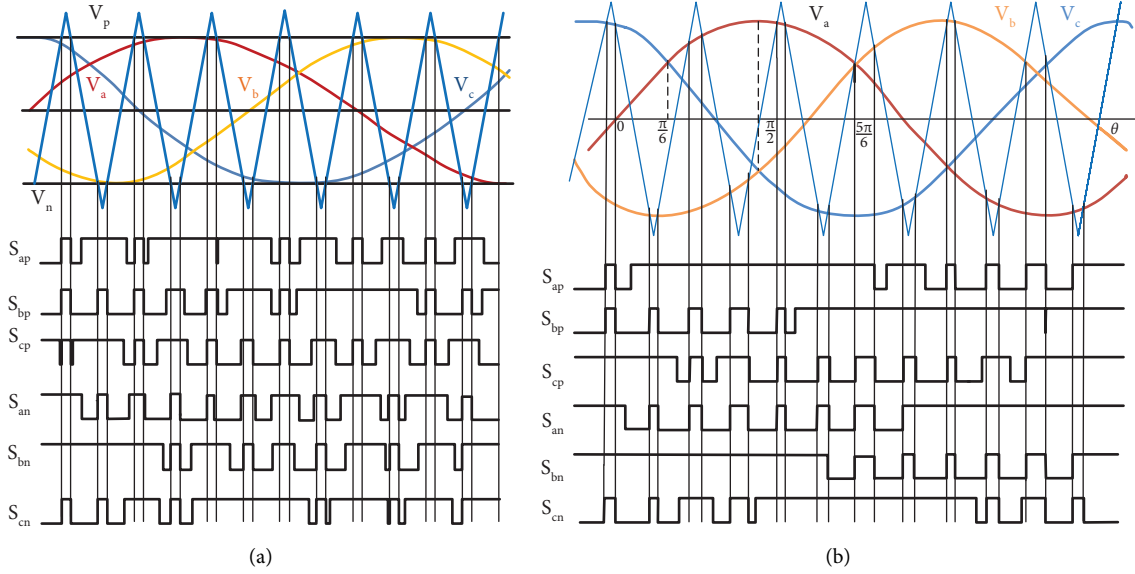


FIGURE 1: Waveforms for (a) simple boost control scheme [4, 6] and (b) maximum boost control scheme [4].

In order to maintain constant gain, one must increase the boost and decrease the modulation index, even vice versa is possible. The gain of the chosen inverter topology is

$$G = \frac{2M - M^2}{2M^2 + M - 2}. \quad (5)$$

The stress across the switches is given by

$$V_S = V_{PN} = BV_{in} = \frac{2(1+D)}{1-5D-2D^2} * V_{in}, \quad (6)$$

where  $V_{pn}$  is the peak-dc link voltage of the inverter (or) voltage across the inverter bridge:

$$V_{pn} = B * V_{in}. \quad (7)$$

In simple boost control [4, 6], the modulation index is limited to  $(1 - D)$ , and if the duty ratio is made to zero, then the modulation index will be one. In order to acquire a higher voltage gain, the  $D$  value must be increased; thus, it leads to reduction in the modulation index, which provides harmonic content in the AC output wave form. Therefore, the maximum boost control technique is proposed in [4] and is analyzed for the presented topology in the following subsection.

**2.2. Maximum Boost Control [4].** But the reduction in the modulation index in the simple boost control scheme leads to greater switch stress as stated in the previous case. Also, to increase the DC bus voltage, the boost factor must be increased which leads to maximization of the duty ratio. The increase in stress reflects to increase in the rating of passive elements ( $L$  and  $C$ ) which increases the size and volume of the converter. To eradicate the abovementioned problem, the maximum boost control technique is introduced in [4].

In MBC, the reference signal is the same as SBC, but the straight lines ( $V_p$  and  $V_n$ ) are exempted. Hence, the carrier signal is compared with the sine wave ( $V_a, V_b, V_c$ ) as well as with the zero reference. As shown in Figure 1(b), if it is greater than the two signals, then only the signal is generated for the shoot-through condition. Under normal instants, the behaviour of the scheme is like carrier PWM; hence, the inverter operates like VSI. This criterion shows that the MBC allows and transforms the zero or null vectors to shoot-through vectors. Thus, maximum on time ( $T_0$ ) and boost factor ( $B$ ) are obtained for any given modulation index value without distorting output waveform. The limitation in this control scheme is that the shoot-through duty cycle is not constant under every instant. This variation in the duty ratio for every cycle is undesirable; hence, the average of the shoot-through duty cycle is considered.

$$D = \int_{\pi/6}^{\pi/2} \frac{2 - (M \cdot \sin \theta - M \cdot \sin(\theta - (2\pi/8)))}{2} d\theta. \quad (8)$$

The shoot-through state repeats periodically every  $60^\circ$ . From the schematic diagram, the frequency of the carrier wave is much higher than the reference.

$$D = \frac{2\pi - 3\sqrt{3}M}{2\pi}. \quad (9)$$

By substituting the abovementioned duty cycle in boost factor (1), the boost factor is obtained for the MBC technique as

$$B = \frac{8\pi^2 - 6\sqrt{3}\pi M}{3\sqrt{3}\pi M - 12\pi^2 - 27M^2}. \quad (10)$$

The voltage stress of the inverter is

$$V_S = BV_{in} = \left( \frac{8\pi^2 - 6\sqrt{3}\pi M}{3\sqrt{3}\pi M - 12\pi^2 - 27M^2} \right) * V_{in}. \quad (11)$$

The gain of the topology is expressed as

$$G = \frac{MB}{2} = \frac{4\pi^2 - 3\sqrt{3}M}{3\sqrt{3}\pi M - 12\pi^2 - 27M^2} \quad (12)$$

**2.3. Maximum Boost Control with Third Harmonic Injection [4].** PWM techniques are the control strategies for all inverters, whereas in ZSI, the traditional PWM does not retain the boost. Hence, to retain the boosting ability, the SBC and MBC techniques are discussed in the previous case. It is observed from the previous analysis that in the case of SBC, the switch stress is increased and the shoot-through duty cycle is limited to  $(1 - M)$ , and these limitations led to introduction of MBC. In the MBC, the stresses are reduced and the gain factor is increased, but the modulation index is limited to 1. Hence, this permits the limitation of this control.

In MBC, the stresses are reduced, but the improvement in the range of the modulation index is not possible. Hence, the third harmonic injection (THI) is introduced [4]. The THI control is similar to MBC. In MBC, a pure sine wave is used for scheme, but in MBC-THI, the  $(1/6)^{th}$  harmonic signal is injected into the reference wave. A harmonic signal whose frequency is three times the fundamental wave is injected into the reference wave. The final wave generated by this criterion is used as the reference signal and is shown in Figure 2(a). The reason behind the injection of a harmonic signal is to enhance the modulation index range to  $M \leq 2/\sqrt{3}$ . The range of the  $M$  is increased; hence, the gain value is increased than MBC comparatively. The synopsis and control are similar to MBC. When the carrier wave is higher than the reference ( $V_a, V_b, V_c$ ), the pulse is generated and the ST state occurs. Since the control is similar, the equivalent shoot-through duty cycle of the scheme is also similar to MBC. Therefore, the shoot-through duty cycle repeats every  $\pi/3$ , and the switching cycle considered for the analysis is in the range of  $\pi/6$  to  $\pi/2$ .

Thus, the average duty cycle of MBC-THI control scheme is derived as [3]

$$D = \int_{\pi/6}^{\pi/2} \frac{2 - (M \sin\theta + (1/6)M \sin 3\theta) - (M \sin(\theta - (2\pi/8)) + (1/6)M \sin 3\theta)}{2} d\theta \quad (13)$$

$$D = \frac{2\pi - 3\sqrt{3}M}{2\pi} \quad (14)$$

From (14), the boost factor for the chosen topology is derived as

$$B = \frac{8\pi^2 - 6\sqrt{3}\pi M}{3\sqrt{3}\pi M - 12\pi^2 - 27M^2} \quad (15)$$

Since the duty ratio is similar, the gain and the voltage stress of the topology are given in the following equations:

$$G = \frac{MB}{2} = \frac{4\pi^2 - 3\sqrt{3}M}{3\sqrt{3}\pi M - 12\pi^2 - 27M^2} \text{ and} \quad (16)$$

$$V_s = BV_{in} = \left( \frac{8\pi^2 - 6\sqrt{3}\pi M}{3\sqrt{3}\pi M - 12\pi^2 - 27M^2} \right) * V_{in} \quad (17)$$

**2.4. Maximum Constant Boost Control [5].** The SBC, MBC, and THI are discussed in [4] that have prior limitations of their own. In SBC, the stresses are increased in MBC; one cannot increase the range of the modulation index; hence, THI was introduced. But in MBC and THI, the shoot-through duty cycle is not constant under every instant. This is the major limitation to be focused on because the variation in “ $D$ ” under every instant leads to variation in the storage capability of the  $L$ - $C$  components. This variation leads to introduction of ripples in the circuit topology. These ripples are caused by the inductor in the output. When the

output frequency is lower than the inductor current, ripple content becomes significant and large inductor is required. To calculate the ripple content, the impedance network is modelled as shown in Figure 3.

$V_{cap}$  is the capacitor voltage in Z-network and  $V_i$  is the input of the topology. Neglecting the switching, frequency element, and the average value of  $V_i$  can be given by the following equation:

$$V_i = (1 - D_o)BV_{dc} \quad (18)$$

From MBC [3], the value of  $D_o$  is

$$D_o(\omega t) = \frac{2 - (M \sin\omega t - M \sin(\omega t - 2(\pi/3)))}{2} \quad (19)$$

$$D_o(\omega t) = 1 - \frac{\sqrt{3}}{2} \cos\left(\omega t - \frac{\pi}{3}\right) \text{ for } \left(\frac{\pi}{6} < \omega t < \frac{\pi}{2}\right) \quad (20)$$

where “ $\omega$ ” is the output angular frequency from the equation mentioned above, and it is seen that  $D_o$  has the maximum value at  $\omega t = (\pi/2)$  (or)  $(\pi/6)$  and it has the minimum value at  $\omega t = (\pi/3)$ . In most of the Z-network topologies, the voltage across the capacitors is considered as a constant, hence considering the same assumptions under this case. The voltage ripples in the inductor are given by  $V_{ripple}$  considering that the ripple is sinusoidal in nature.

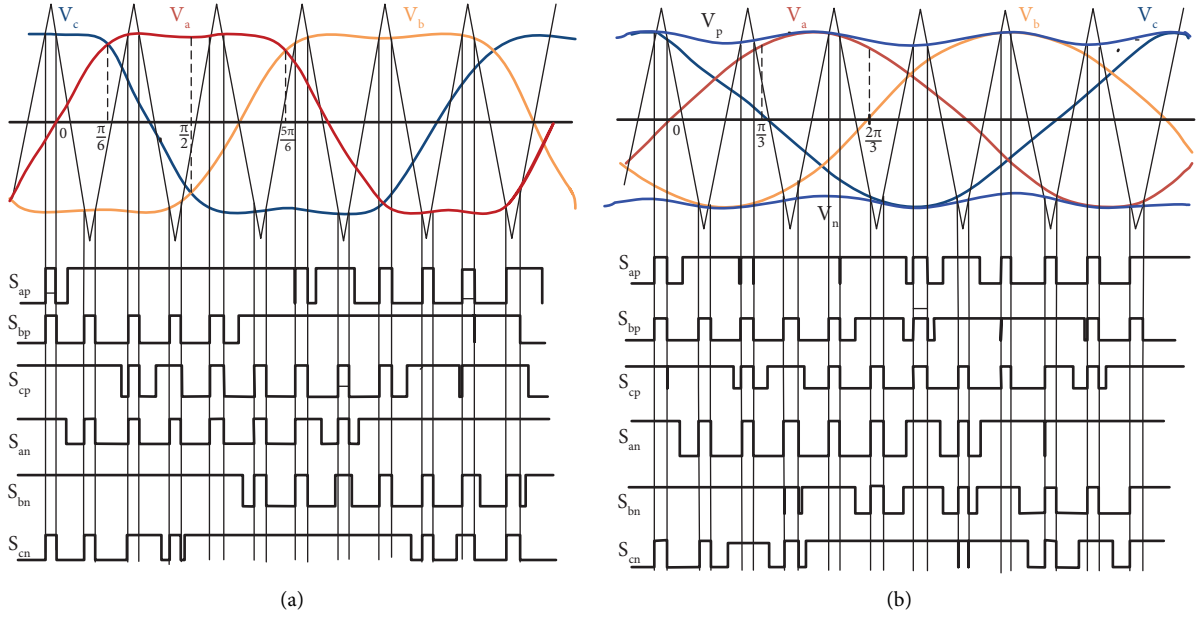


FIGURE 2: Waveforms for (a) third harmonic injection control scheme [4] and (b) maximum constant boost control scheme [5].

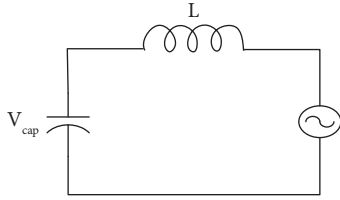


FIGURE 3: Equivalent of Z-network for maximum boost control [4].

$$V_{\text{ripple}} = V_{\text{imax}} - V_{\text{imin}},$$

$$V_{\text{ripple}} = \left( \frac{\sqrt{3}}{2} M - \frac{\sqrt{3}}{2} M \cos\left(\frac{\pi}{6}\right) \right) * BV_{\text{dc}}. \quad (21)$$

Thus, the ripple currents in the inductor are

$$\Delta I_L = \frac{V_r}{6\omega L}. \quad (22)$$

From the abovementioned expression, it is clear that the inductor value has to be large for low output frequency in order to limit current ripple within a certain range. Thus, MBC is in application where high output frequency and current ripple do not interfere (or) distort the output. In order to eradicate the abovementioned problem, constant boost control (MCBC) is introduced as shown in Figure 2(b) [5].

In the MCBC, the main motto is to get constant boost, under every instant which eliminates the ripples. In this scheme, the reference signal is the sine signal ( $V_a$ ,  $V_b$ ,  $V_c$ ) enclosed by two envelope signals ( $V_p$ ,  $V_n$ ). Thus, there are five signals embedded in it. When the carried triangular signal is higher than the sine wave and the envelope signal,

then the pulse is generated to initiate ST condition under other instants, and it operates as a traditional inverter. The envelope curves are sinusoidal in nature, and they are of frequency three times the fundamental sine wave. This has two half periods for both curves in a cycle. For the first half period, the upper and lower envelope signal is turned as

$$V_{p1} = \sqrt{3}M + \sin\left(\theta - 2\frac{\pi}{3}\right)M, \quad \text{for } \left(0 < \theta < \frac{\pi}{3}\right), \quad (23)$$

$$V_{n1} = \sin\left(\theta - 2\frac{\pi}{3}\right)M, \quad \text{for } \left(0 < \theta < \frac{\pi}{3}\right). \quad (24)$$

For the second half period  $[\pi/3, 2\pi/3]$ , the enveloped curves are termed as

$$V_{p2} = \sin(\theta)M, \quad \text{for } \left(\frac{\pi}{3} < \theta < 2\frac{\pi}{3}\right), \quad (25)$$

$$V_{n2} = \sin(\theta)M - \sqrt{3}M, \quad \text{for } \left(\frac{\pi}{3} < \theta < 2\frac{\pi}{3}\right). \quad (26)$$

The distance between the two envelope curves is given by  $\sqrt{3}M$ , where  $M$  is the modulation index and the shoot-through duty ratio is also constant all the time. The duty ratio can be expressed by

$$D = \frac{2 - \sqrt{3}M}{2}. \quad (27)$$

From abovementioned equation, the boost factor of the topology is

$$B = \frac{\sqrt{3}M - 4}{6M^2 - 14\sqrt{3}M + 8}. \quad (28)$$

The voltage stress and gain of the inverter topology are

$$V_s = BV_{in} = \left( \frac{\sqrt{3}M - 4}{6M^2 - 14\sqrt{3}M + 8} \right) * V_{in} \text{ and} \quad (29)$$

$$G = \frac{\sqrt{3}/2M - 2}{6M^2 - 14\sqrt{3}M + 8}. \quad (30)$$

From the above, it is seen that the shoot-through state appears when it carries higher/lower than the reference and envelope signals. Under other instants, the scheme behaves as a traditional PWM scheme maintaining the boost constant, which is possible by maintaining the value “ $D$ ” constant. The abovementioned control is advantageous for two cases to reduce stress and maintain the boost constant. This scheme can be modified further by combining third harmonic injection control in it. This increases the range of  $M$ . Hence, the constant boost control with the third harmonic injection was introduced [5] and is shown in Figure 4.

**2.5. Constant Boost Control with the Third Harmonic Injection.** In the previous case, the shoot-through duty ratio is always constant. For a modulation index  $M$ , the maximum active state duty ratio  $D_{a_{max}}$  can be expressed as

$$D_{a_{max}} = \max \left( \frac{M \sin \omega t - M \sin (\omega t - 2(\pi/3))}{2} \right). \quad (31)$$

If the active states are unchanged, by making the boost and duty ratio constant, then the resultant maximum shoot-through duty ratio acquired is

$$\begin{aligned} D_{0_{max}} &= 1 - D_{a_{max}} \\ &= 1 - \frac{\sqrt{3}}{2}M. \end{aligned} \quad (32)$$

It is seen that the modulation index is limited under this scheme. Hence, constant boost control with the third harmonic injection (CBC-THI) is introduced. This control is similar to the pervious scheme, but the modulation signals are differed, and in this case, a third harmonic component with  $1/6^{\text{th}}$  of the fundamental frequency is injected into the sinusoidal signal. The resultant signal generated is used as reference ( $V_a, V_b, V_c$ ).

The scheme is not complete without the envelope signals. ( $V_p, V_n$ ) used in this case are two straight lines. These envelope signals travel tangentially to the surface of the reference signal. When the carrier signal is higher/lower than these reference and envelope signals, then the ST condition is created. The idea here is to increase the modulation index that is done by modulating the reference wave from one form to other. The control and synopsis are similar to the previous case. Hence, the duty ratio is also the same.

$$D = 1 - \frac{\sqrt{3}}{2}M. \quad (33)$$

Hence, the boost factor of the topology is

$$B = \frac{\sqrt{3}M - 4}{6M^2 - 14\sqrt{3}M + 8}. \quad (34)$$

The voltage stress is

$$V_s = BV_{in} = \left( \frac{\sqrt{3}M - 4}{6M^2 - 18\sqrt{3}M + 24} \right) * V_{in}. \quad (35)$$

The gain of the inverter is

$$G = \frac{\sqrt{3}/2M - 2}{6M^2 - 14\sqrt{3}M + 8}. \quad (36)$$

The major advantage in this control is “ $M$ ” value which is increased to  $2/\sqrt{3}$ , since the THI control is embedded in it. Hence, the gain of the topology increases maintaining the boost constant. On the other hand, the control is also similar to SBC since the sine wave is modulated.

### 3. Comparative Analysis for the PWM Techniques

In this section, the comparative analyses between five PWM techniques are discussed. Parameters such as duty ratio ( $D$ ), boost factor ( $B$ ), gain ( $G$ ), and stresses ( $V_s$ ) are compared with the modulation index,  $M$ , for EUHG-qZSI. The clear vision of the abovementioned idea is discussed in detail in the subsection accordingly.

**3.1. Comparison of Duty Ratio and Boost Factor with the Modulation Index.** The first comparison in this analysis is the duty ratio,  $D$ , versus the modulation index,  $M$ . From the previous analyses and derivation, the relation between the modulation index for SBC, MBC, and MCBC is expressed in (3), (9), (14), (27), and (33). Based on these relations, the plot is drawn and depicted in Figure 5(a).

The second comparison (Figure 5(b)) is between the boost factor and the modulation index. This graph is obtained from equations (4), (10), (15), (28), and (34) derived during the analysis in the previous section. This plot gives the variation in  $M$  with respect  $B$ , and it is observed that the relation is hyperbolic in nature, and for every value of the boost factor, the modulation index is decreasing from its maximum value. This plot is for all techniques, and it is observed that the maximum boost control has reliable characteristics among all of them.

**3.2. Relation between Stress and Gain versus Modulation Index.** The voltage stresses are the component potentials appearing across the inverter switches. When the inverter bridge terminal is under ST condition, the energy is stored in passive components, and this stored energy appears as the stress across the devices under normal operation of any topology. The fourth comparison shown in Figure 6(a) is the relation between voltage stress and modulation index. This comparison is attained by using equations (6), (11), (17), (29), and (35) derived during analysis in Section 2. The characteristics are rectangular hyperbolic in nature. In any topology, when the value of  $M$  decreases which leads to

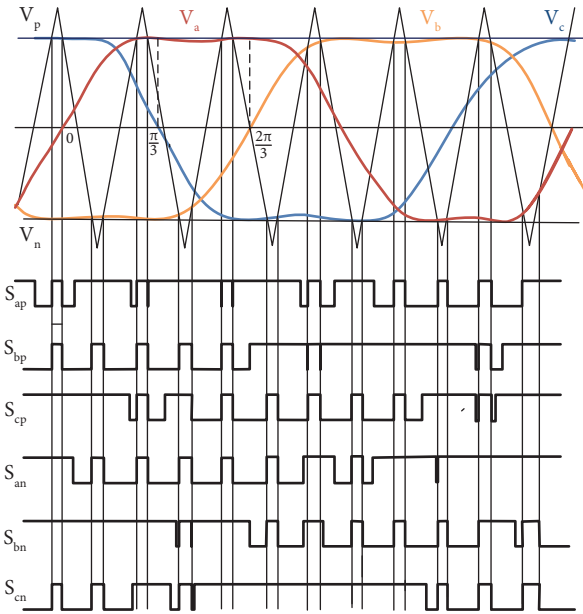


FIGURE 4: Waveforms for constant boost control with the third harmonic injection scheme [5].

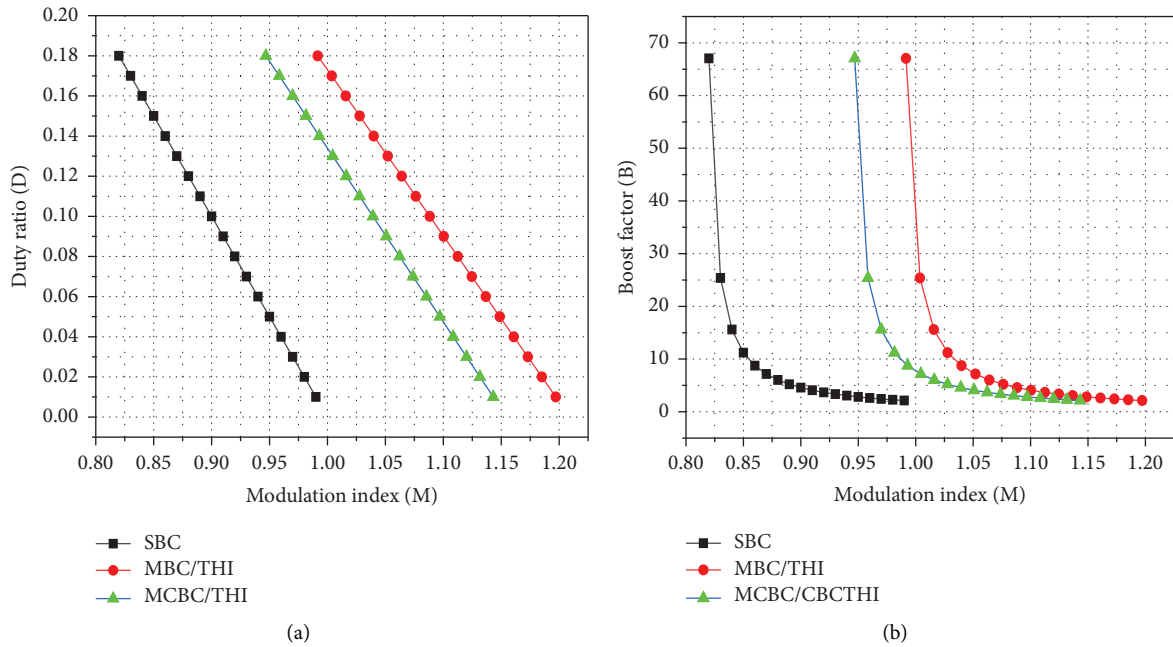


FIGURE 5: Sketch map for various PWM techniques: (a) duty versus modulation index and (b) boost factor versus modulation index.

increase in stress, this statement proves that  $V_s$  and  $M$  are inversely proportional. When SBC is applied, the magnitude of voltage stress is higher, and for MCBC and CBC-THI techniques, they are comparatively lower. When compared to the other MBC technique which has lower stresses, this does not affect the operation, device ratings, and the size and volume of the circuit are also reduced. Figure 7(a) presents the sketch map for various PWM techniques under stress versus modulation index, while Figure 7(b) presents the sketch map for various PWM techniques under gain versus modulation index.

Gain is the product of boost factor and modulation index, and when the boost factor is constant, the gain and modulation index are directly proportional to each other. But the boost varies with the variation in  $D$ , if  $D$  is varied, then  $B$  varies. Hence, the gain depends on  $M$  and  $B$  mainly. The sketch map shown in Figure 6(b) is drawn by using equations (5), (12), (16), (30), and (36) obtained in the abovementioned section. In earlier cases, the characteristics are hyperbolic in nature and the same is repeated in this comparison. But from the comparison, it is observed that gain from SBC scheme is lower from other. All of the above MBC schemes have higher

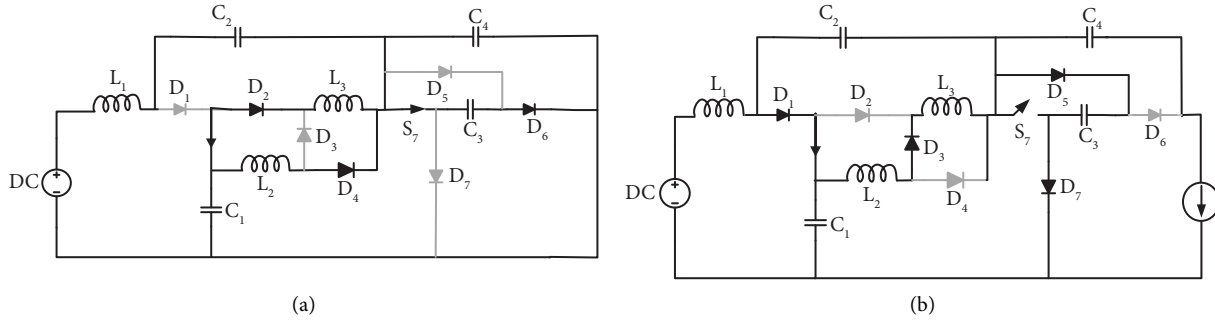


FIGURE 6: Equivalent circuits of EUHG-qZSI under (a) shoot-through state and (b) non-shoot-through state [7].

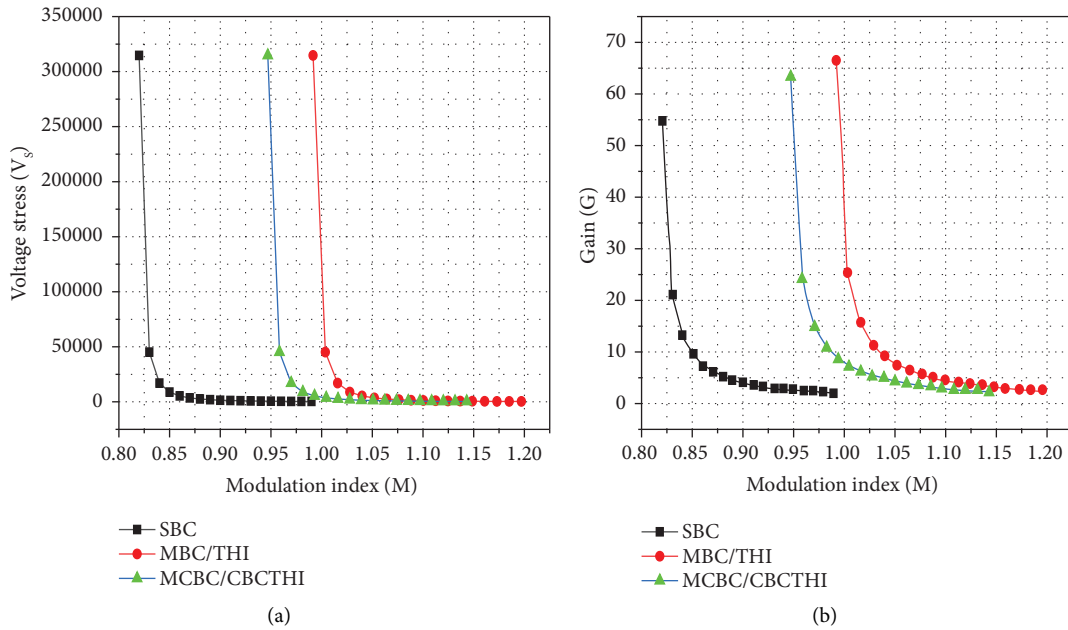


FIGURE 7: Sketch map for various PWM techniques: (a) stress versus modulation index and (b) gain versus modulation index.

gain comparatively. The operating region of the inverter topology is also improved with the improvement in gain. The maximum region is covered by MBC scheme. This proves that MBC is best among all the schemes, and this control is implemented in the simulation also.

Simulation results are shown in Figure 8. This topology uses an  $L$  cell and  $C$  cell network for the boosting terminology. The topology uses a DC source which is the input provided either from the fuel cell stack or a battery pack. The circuit comprises an inductor in series with the source which provides the continuous input current and reduces the ripple. Next to this, the inductor cell is present and these inductors are interconnected through diodes. The circuit comprises of an active switch  $S_7$  in the middle of the  $L$ - $C$  cells. When there is a shoot-through in the circuit, the switch  $S_7$  must be in ON condition; else, the boosting network or the gain does not come into the scenario.

**3.2.1. Principle of Operation for the Presented Topology.** In this paper, an enhanced ultrahigh gain active-switched quasi-Z-source inverter topology is considered for analysis and is depicted in Figure 9.

(1) Shoot-through mode: Figure 6(a) shows the equivalent circuit of the chosen topology. In this mode, all the switches are turned ON (i.e.,  $S_1$  to  $S_7$ ); this helps the inductor cell to store the energy. The diode  $D_1$  is reverse biased as capacitor  $C_2$  applies negative voltage across it. The diode  $D_3$  is OFF as  $L_3$  applies negative voltage across it. The passive components  $L_1$ ,  $L_2$ , and  $C_3$  are in the charging state, and they store the energy. The elements  $C_1$ ,  $C_2$ , and  $C_4$  are discharging.

(2) Non-shoot-through mode: Figure 6(b) shows the equivalent circuit of the chosen topology. In this state, the inverter input is fed to the output. Under this condition, the boost from the previous state and also the input appear across the load.



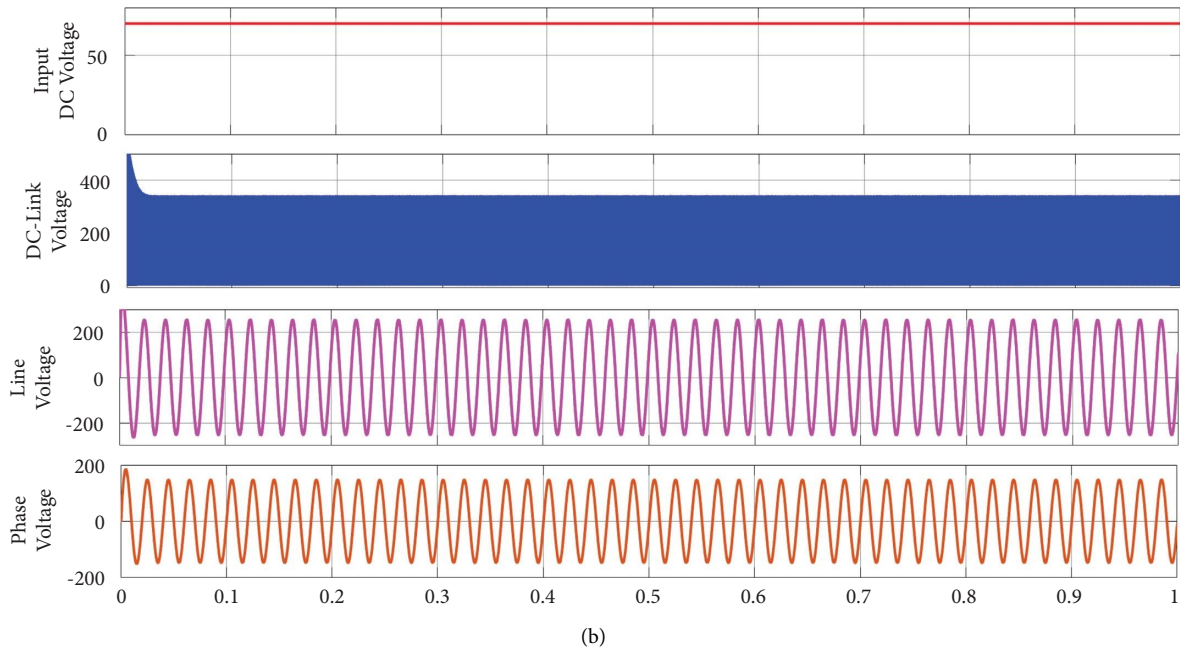
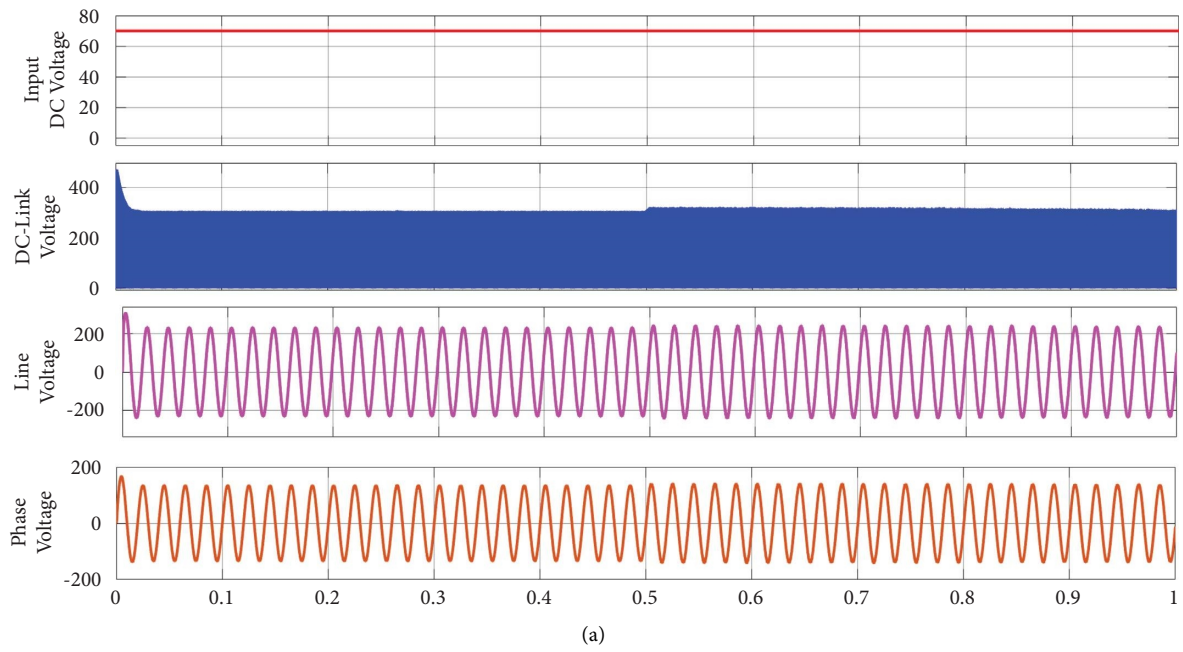
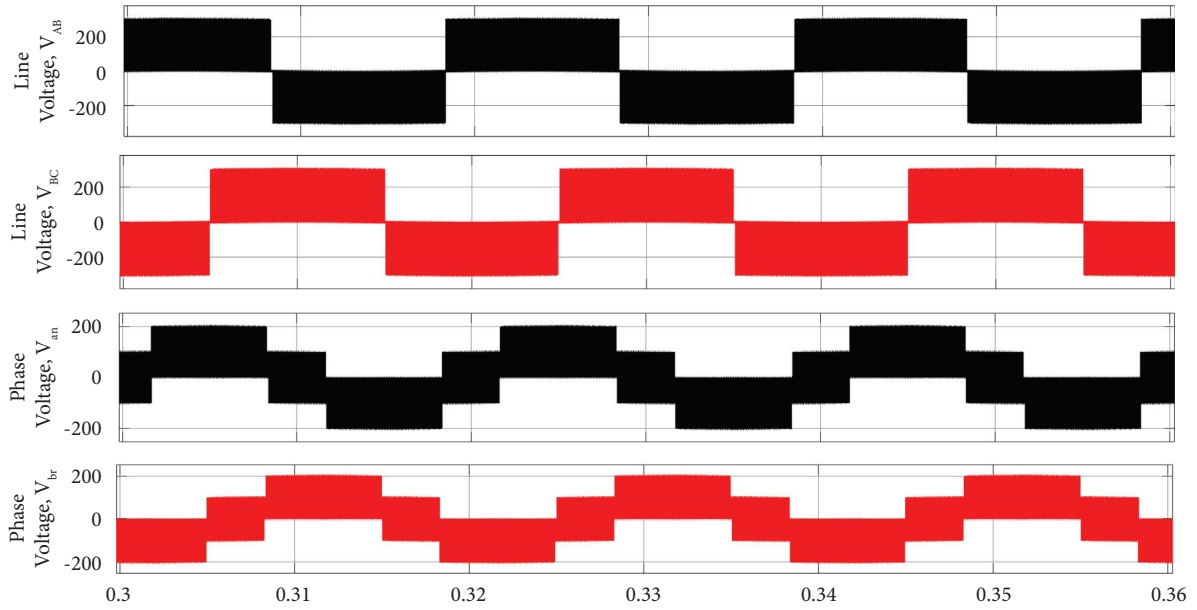
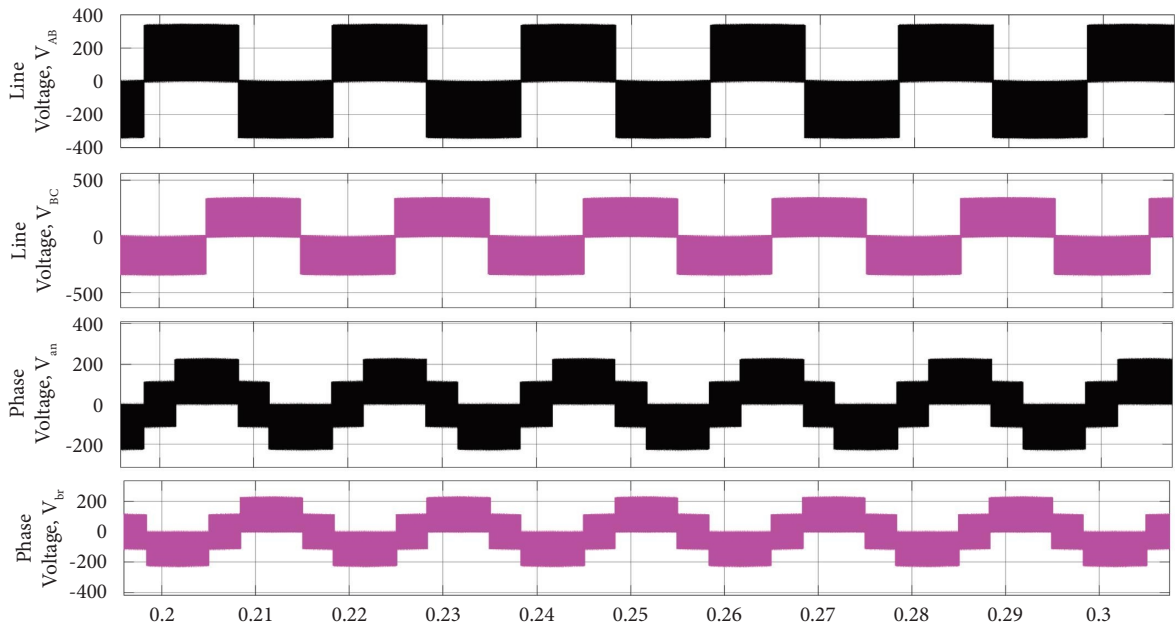


FIGURE 8: Continued.



(c)



(d)

FIGURE 8: Simulation results for input voltage, DC-link voltage, line, and phase voltages with filter for (a) MCBC PWM technique and (b) MBC PWM technique and line voltages and phase voltages without filters for (c) MCBC PWM technique and (d) MBC PWM technique.

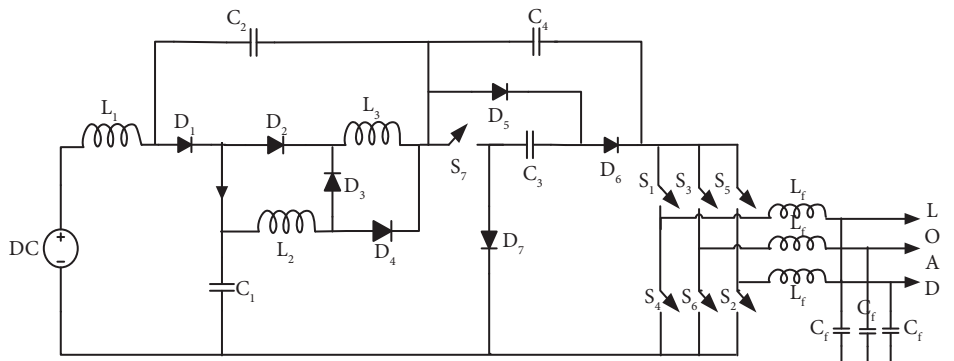
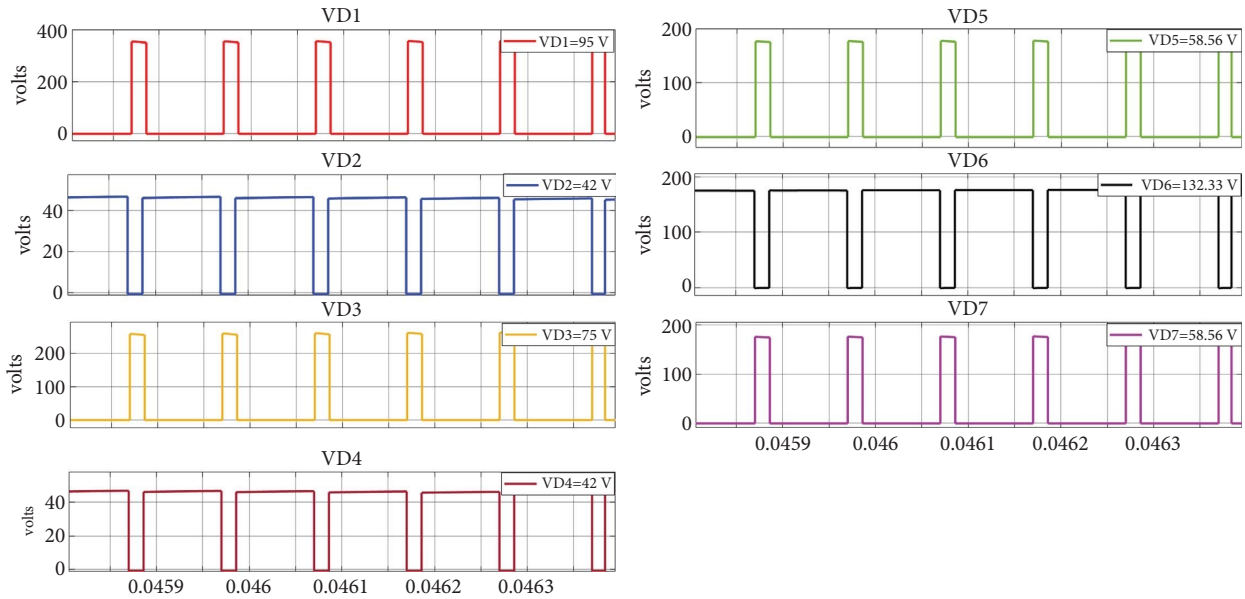


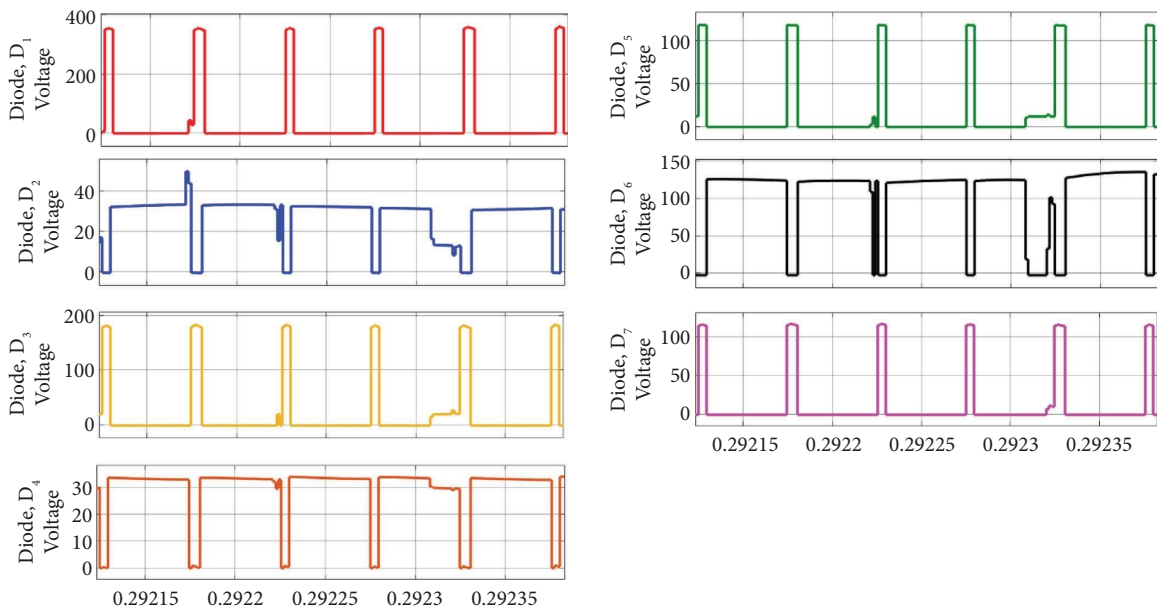
FIGURE 9: Enhanced ultra-high gain active-switched quasi-Z-source inverter [7].

TABLE 1: Inverter Input and output parameters.

$D = 0.1, V_{in} = 70 \text{ V}, B = 4.583 \text{ (MCBC)}$			
Theoretical	1.03 (M)	320.1 V (Vdc link)	128.4 V (V-line)
Simulated	1.03 (M)	318.6 V (Vdc link)	126.4 V (V-line)
$D = 0.1, V_{in} = 70 \text{ V}, B = 4.583 \text{ (MBC)}$			
Theoretical	1.088 (M)	345 V (Vdc link)	317 V (V-line)
Simulated	1.088 (M)	344.7 V (Vdc link)	315.9 V (V-line)



(a)



(b)

FIGURE 10: Continued.

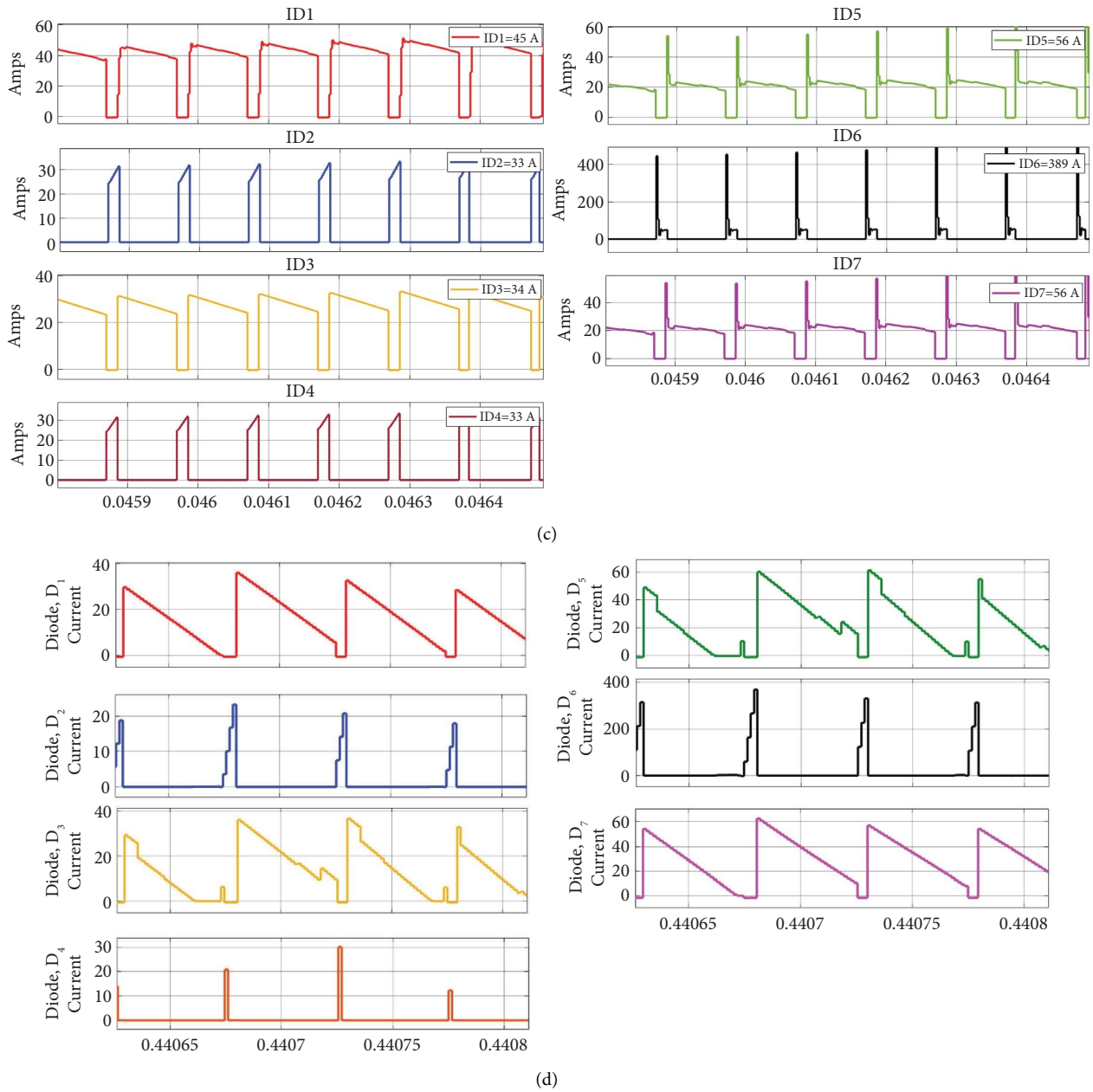


FIGURE 10: Simulation results of diodes ( $D_1$ ,  $D_2$ ,  $D_3$ ,  $D_4$ ,  $D_5$ ,  $D_6$ , and  $D_7$ ) voltages for (a) MCBC PWM technique and (b) MBC PWM technique and diodes ( $D_1$ ,  $D_2$ ,  $D_3$ ,  $D_4$ ,  $D_5$ ,  $D_6$ , and  $D_7$ ) currents (bottom) for (c) MCBC PWM technique and (d) MBC PWM technique.

The diodes  $D_1$  and  $D_3$  are in ON condition and the diodes  $D_2$  and  $D_4$  are OFF, which make the inductors to appear in series with each other.  $L_1$ ,  $L_2$ , and  $C_3$  are in the charging state, whereas  $C_1$ ,  $C_2$ , and  $C_4$  are in the discharging state accordingly.

#### 4. Simulations and Results

To verify the presented PWM techniques, the simulations were conducted for the topology shown in Figure 6. The applied PWM technique presented in EUHG-qZSI [7] analysis is compared with the MBC PWM technique. The simulations were executed for the following parameters:  $L_1 = 1$  mH,  $L_2 = L_3 = 0.5$  mH,  $C_1 = C_2 = C_3 = C_4 = 470$   $\mu$ F, and

switching frequency = 10 kHz, for an  $R$ - $L$  load. The resistance value is chosen as 50  $\Omega$  and inductance value of 60 mH. This load is connected through an  $L$ - $C$  filter with an inductance of 2 mH and capacitance of 50  $\mu$ F. The simulation results with a similar duty ratio  $D = 0.1$  and a modulation index  $M = 1.03$  for MCBC strategy and  $M = 1.088$  for MBC strategy are shown in Figures 8(a) and 8(b), respectively, where the input voltage is 70 V.

The simulations were carried using MATLAB/Simulink. This is used for virtual simulation of the circuits. First, the simulations were performed with the MCBC [5] control strategy to the presented topology. The parameters chosen for the MCBC and MBC are shown in Table 1.

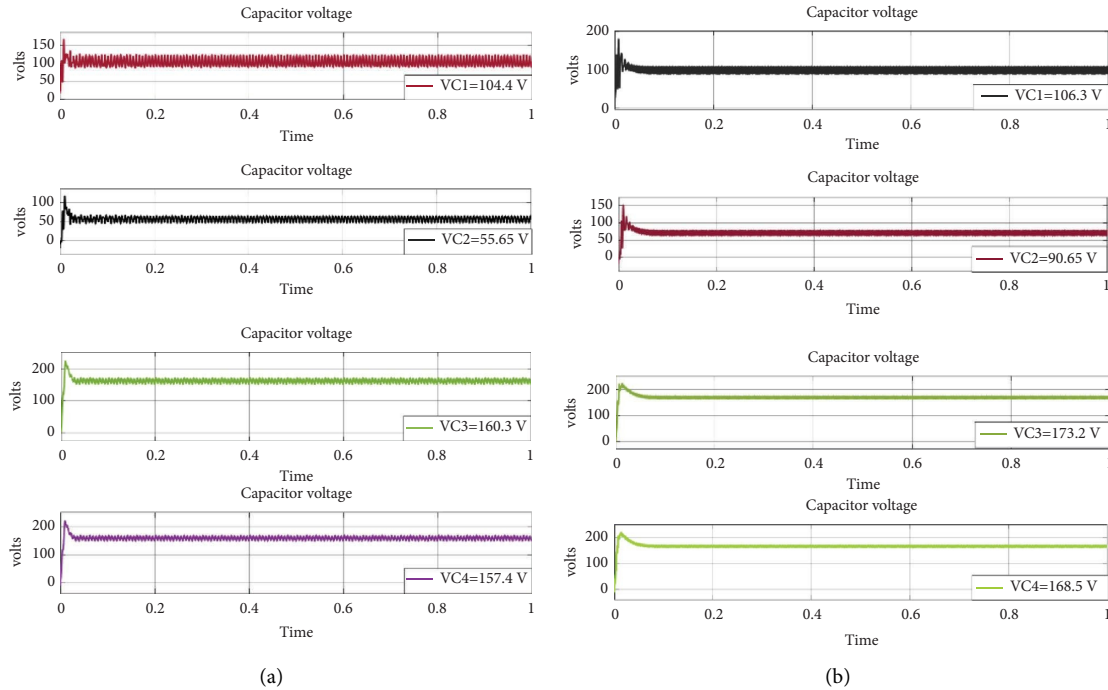


FIGURE 11: Simulation results of EUHG-qZSI capacitor stresses for (a) MCBC PWM technique and (b) MBC PWM technique.

The simulation results are shown in Figure 8(a), which resemble the inverter output parameters for the MCBC PWM technique. The input provided to the inverter was 70 V DC voltage, and the acquired output DC link voltage is 319.1 V. Thus, the simulation results are approximately consistent with the theoretical analysis. Hence, the same must be implemented for the MBC PWM strategy also.

The simulation results shown in Figure 8(b) resemble the inverter output parameters for the MBC PWM technique. The input provided to the inverter was 70 V DC voltage, and the acquired output DC link voltage is 344.7 V. Thus, the simulation results are approximately consistent with the theoretical analysis. It is observed from Figures 8(c) and 8(d) that for the same input voltage and duty cycle, the DC-link voltage is more in the MBC PWM technique. Due to this, the AC output voltages provide more in the case of MBC PWM. The change in output voltage is due to the change in the voltage gain value. Hence, it is observed that the gain in the MBC PWM is more in compensation of lower voltage stress across the inverter bridge.

The overall voltage stress on diodes will be less for the MBC PWM technique when compared to the MCBC PWM technique which can be observed from Figure 10.

Figures 11(a) and 11(b) show the capacitor voltages of the chosen topology. Theoretical values for capacitors  $C_1$ ,  $C_2$ , and  $C_3/C_4$  are obtained as 105.08 V, 60.03 V, and 161.41 V, respectively, for MCBC control scheme and the simulated values are acquired as 104.4 V, 55.65 V, 160.3 V, and 157.4 V. The simulation values are matching the theoretical values. Similarly, theoretical values of the capacitor voltages for the MBC PWM strategy are acquired as 107.8 V, 91.79 V, 174.1 V, and 169.7 V, respectively, and the simulated values are obtained as 106.3 V, 90.65 V, 173.3 V, and 168.5 V,

respectively. These simulated values are also matching with the theoretical values obtained. In MCBC PWM, the output voltage and the gain value are comparatively lower due to the reduction in capacitor stresses. This criterion is appearing due to the control scheme implemented. Likewise, in MBC PWM, the voltage stress or the bridge stresses are reduced rather than the capacitor stress. Thus, if the inverter is used for high voltage gain applications, then MBC PWM is the most feasible of the five illustrated above.

## 5. Conclusion

This paper presents five pulse-width modulated (PWM) control strategies introduced in the earlier times, and those are simple boost control (SBC), maximum boost control (MBC), third harmonic injection (THI), maximum constant boost control (MCBC), and constant boost control with third harmonic injection (CBC-THI). All these control techniques were applied to the novel EUHG-qZSI topology. These PWM techniques are analyzed, and it was concluded that the maximum boost control (MBC) gives better performance. This is also proven with the theoretical and simulation test verification.

## Data Availability

The data used to support the findings of this study are available from the corresponding author upon request.

## Conflicts of Interest

The authors declare that they have no conflicts of interest.

## References

- [1] N. Mohan, T. M. Undeland, and W. P. Robbins, *Power Electronics: Converters, Applications, and Design*, Wiley, New York, NY, USA, 1995.
- [2] G. Ledwich, "Current source inverter modulation," *IEEE Transactions on Power Electronics*, vol. 6, no. 4, pp. 618–623, 1991.
- [3] F. Z. Peng, "Z-source inverter," *IEEE Transactions on Industry Applications*, vol. 39, no. 2, pp. 504–510, 2003.
- [4] F. Z. Peng, M. Shen, and Z. Qian, "Maximum boost control of the Zsource inverter," *IEEE Transactions on Power Electronics*, vol. 20, no. 4, pp. 833–838, 2005.
- [5] F. Z. Peng, M. Shen, A. Joseph, Fang Zheng Peng, L. Tolbert, and D. Adams, "Constant boost control of the Z-source inverter to minimize CurrentRipple and voltage stress," *IEEE Transactions on Industry Applications*, vol. 42, no. 3, pp. 770–778, 2006.
- [6] V. Jagan, J. Kotturu, and S. Das, "Enhanced-boost quasi-Z-source inverters with two-switched impedance networks," *IEEE Transactions on Industry Applications*, vol. 64, no. 9, pp. 6885–6897, 2017.
- [7] P. K. Gayen and S. Das, "An enhanced ultra-high gain active-switched quasi Z-source inverter," *IEEE Transactions on Circuits and Systems II: Express Briefs*, vol. 69, no. 3, pp. 1517–1521, 2022.
- [8] M. Zhu, Kun Yu, and Fang Lin Luo, "Switched inductor Z-source inverter," *IEEE Transactions on Power Electronics*, vol. 25, no. 8, pp. 2150–2158, 2010.
- [9] Y. P. Siwakoti, P. C. Loh, F. Blaabjerg, and G. E. Town, "Y-source impedance network," *IEEE Transactions on Power Electronics*, vol. 29, no. 7, pp. 3250–3254, 2014.
- [10] S. Xie, Y. Tang, and C. Zhang, "Research on third harmonic injection control strategy of improved Z-source inverter," in *Proceedings of the 2009 IEEE Energy Conversion Congress and Exposition*, San Jose, CA, USA, September 2009.
- [11] W. Xu, M. Liu, J. Liu, K. W. Chan, and K. W. E. Cheng, "A series of new control methods for single-phase Z-source inverters and the optimized operation," *IEEE Access*, vol. 7, pp. 113786–113800, 2019.
- [12] W. Liu, Y. Yang, T. Kerekes, D. Vinnikov, and F. Blaabjerg, "Inductor current ripple analysis and reduction for quasi-Z-source inverters with an improved ZSVM6 strategy," *IEEE Transactions on Power Electronics*, vol. 36, no. 7, pp. 7693–7704, 2021.
- [13] P. Liu, J. Xu, M. Sun, J. Yuan, and F. Blaabjerg, "New discontinuous space vector modulation strategies for impedance-source inverter with superior thermal and harmonic performance," *IEEE Transactions on Industrial Electronics*, vol. 69, no. 12, pp. 13079–13089, 2022.
- [14] X. Zhu, K. Ye, L. Jiang, K. Jin, W. Zhou, and B. Zhang, "Nonisolated single-phase quadratic switched-boost inverter with continuous input current and step-up inversion capability," *IEEE Journal of Emerging and Selected Topics in Industrial Electronics*, vol. 4, no. 1, pp. 276–287, 2023.
- [15] V. Jagan, M. Bhavadish Chary, M. Sankeerthana, K. Aishwarya, S. Nikhil, and K. Deepika, "A superior boost active-switched impedance network quasi Z-source inverter," in *Proceedings of the IEEE Int. Conf. on Computer, Electronics and Electrical Eng. and Their Appl. (IC2E3-2023)*, NIT-Uttarakhand, Srinagar Garhwal, India, June, 2023.
- [16] B. Nagi Reddy, B. Sai Kumar, B. Sai Sri Vindhya et al., "Switched quasi impedance-source DC-DC network for photovoltaic systems," *International Journal of Renewable Energy Resources*, vol. 13, no. 2, 2023.
- [17] V. Jagan, B. C. Maheshwaram, M. Usirikapally, S. Mettu, A. Kusumba, and N. Sriramoju, "Analysis of conventional PWM techniques for enhanced ultra high gain Z-network," in *Proceedings of the 2023 International Conference on Computer, Electronics & Electrical Engineering & their Applications (IC2E3)*, pp. 1–6, Srinagar Garhwal, India, June 2023.
- [18] V. Jagan, S. Das, A. Mithun Kumar Reddy, C. Swetha, and M. Neeharika, "A family of switched-impedance network enhanced-boost quasi-Z-source inverters," *International Journal of Power Electronics and Drive Systems*, vol. 13, no. 1, pp. 309–321, 2022.